ISSN 0001-4338, Izvestiya, Atmospheric and Oceanic Physics, 2020, Vol. 56, No. 4, pp. 378–389. © Pleiades Publishing, Ltd., 2020.
Russian Text © The Author(s), 2020, published in Izvestiya Rossiiskoi Akademii Nauk, Fizika Atmosfery i Okeana, 2020, Vol. 56, No. 4, pp. 433–445.

Dynamics of Zonally Averaged Circulation Characteristics in the Middle Atmosphere

O. S. Zorkaltseva[a, b, *], V. I. Mordvinov[a], A. I. Pogoreltsev[c, d], and N. S. Dombrovskaya[a]

[a] *Institute of Solar-Terrestrial Physics, Siberian Branch, Russian Academy of Sciences, Irkutsk, 664033 Russia*
[b] *Irkutsk State University, Irkutsk, 664033 Russia*
[c] *Russian State Hydrometeorological University, St. Petersburg, 195196 Russia*
[d] *St. Petersburg State University, Peterhof, 198504 Russia*
**e-mail: olgak@mail.iszf.irk.ru*

Received September 26, 2019; revised January 29, 2020; accepted February 5, 2020

Abstract—The ERA-Interim archive data and circulation calculations using a middle and upper atmosphere model (MUAM) have been used to study dynamic processes in the middle atmosphere. Variations in zonally averaged atmospheric characteristics have been analyzed based on observational data and model calculations. In the middle atmosphere within a range of 10–30 days, synchronous temperature variations are observed within zones extended horizontally and vertically. Horizontally, the sign of such variations changes in the region of jet streams (and remains unchanged at the equator) and, vertically, their sign changes within the stratopause and mesopause regions. The nature of these variations is almost independent of the phase of the quasi-biennial cycle in the equatorial stratosphere. These variations are global in nature and similar to oscillations in meridional circulation cells.

Keywords: stratosphere, mesosphere, sudden stratospheric warming, quasi-biennial oscillation
DOI: 10.1134/S0001433820040118

1. INTRODUCTION

The low-frequency atmospheric variability within periods of 10–30 days includes variations caused by traveling Rossby waves, quasi-stationary waves associated with both orographic and thermal anomalies, and nonlinear interactions [1, 2]. One of the most complex dynamic phenomena in the middle atmosphere is a sudden stratospheric warming (SSW) [3–5], during which the polar vortex breaks down. In this case, in the high latitudes, the air temperature may rise several tens of degrees. Throughout almost the entire middle-atmosphere thickness, zonally averaged meteorological parameters (such as velocity, temperature, etc.) that characterize the polar vortex dynamics significantly vary and both thermal and baric anomalies increase along latitude circles. One can morphologically represent the SSW as a result of the dynamic interaction between the polar cyclonic vortex and one or a few anticyclonic vortices in the middle atmosphere [6].

The SSW is associated with intrinsic instabilities of jet streams in the middle atmosphere [7–9] or with external factors, such as stationary planetary waves propagating from the troposphere, blockings, and disturbances caused by convective processes in the tropics [3, 6, 10]. However, it is unclear to what extent these mechanisms are related, whether the SSW is, to a greater extent, an explosive amplification of natural oscillations in the middle atmosphere or a result of external energy transportation and interaction of waves and vortices with the mean flow.

Zonal averagings that make it possible to isolate the life cycle of disturbances and study their relation to external factors and background quasiregular oscillations in the middle atmosphere are a convenient diagnostic method of studying dynamic processes. It is known that zonally averaged characteristics vary within a wide frequency range (from seasonal to diurnal variations) [11]. Such variations within a period of 40–50 days are usually associated with orographic excitation [12] and the Madden–Julian oscillation [11, 13]; the 10- to 30-day interval has been much less studied.

Current reanalysis archive data may be used in studying oscillations in the stratosphere and lower mesosphere. Model calculations are necessary to study processes in the upper mesosphere and lower thermosphere. To this end, a middle and upper atmosphere model (MUAM) [15] was used in [14]. Such calculations reproduced a lot of regularities in the distribution and dynamics of zonally averaged circulation characteristics during SSWs at different phases of the quasi-biennial oscillation (QBO) and the Madden–Julian oscillation. It is particularly important that such

model calculations make it possible to monitor external factors that may generate not only quasiregular oscillations in the upper atmosphere, but also explosive processes of the SSW type.

The MUAM model and the scheme of numerical experiments are described in Section 2. The QBO effect was specified using an additional term in a prognostic equation. Calculation results were compared with the ERA-Interim archive data individually for the western and eastern phases of the QBO in different latitudinal zones and at different atmospheric heights. Both trends and high-frequency oscillations were eliminated using moving average windows of 10 and 30 days. In order to analyze the propagation of disturbances both vertically and meridionally, the latitude–time and height–time diagrams and the curves of cross-correlation between variations in zonally averaged velocity and temperature in different latitudinal zones and at different atmospheric levels were plotted. Section 3 gives the results of calculations of cross-correlation curves on the basis of the ERA-Interim data and model calculations. The degree of agreement between observational and model data and the features of distributions of cross-correlation curves are analyzed.

2. DESCRIPTION OF MODEL EXPERIMENTS

2.1. Simulation Method

The three-dimensional nonlinear MUAM (within a height range of 0–300 km) implemented on a grid of size 5.625° in longitude and 5° in latitude and with 56 height levels [15] was used to simulate the thermal regime and general circulation of the atmosphere. The integration time step was 225 s. The last MUAM version included a new parameterization of the effects of orographic gravity waves [16] and new climatic distributions of ozone [17] and water vapor in the troposphere [18], which take into account the longitude dependence. The dimensionless log-isobaric height $x = -\ln(p/1000)$, where p is pressure in hPa, is a vertical coordinate of the model. The lower boundary conditions at a level of 1000 hPa are the geopotential-height and temperature distributions in January, which take into account zonally averaged values and stationary planetary waves with zonal wavenumbers $m = 1–5$. The Japanese reanalysis (JRA55) data [19] for the neutral phase of the El Nino–Southern Oscillation (ENSO) according to the Multivariate ENSO Index (MEI) were used to eliminate the influence of the ENSO phenomenon in calculating the lower boundary conditions.

The QBO effect was specified by an additional term in the prognostic equation for the zonal velocity component, which is proportional to the difference between calculated and climatic distributions of zonally averaged wind velocity values for the western and eastern phases of the QBO. The additional term was introduced within a latitude interval of 17.5° S–17.5° N at heights of 0–50 km. The characteristic time of "attraction" of the model zonally averaged flow to the MERRA reanalysis data was 5 days.

2.2. Scheme of Numerical Experiments

Numerical experiments were carried out individually for the eastern and western phases of the QBO. The length of each realization was 400 model days. During the first 120 days, only a daily mean warming of the atmosphere was taken into account. Daily warming variations and an additional equation for geopotential disturbances at the lower boundary of the calculation domain were gradually introduced from the 121st day to the 330th day. From the 331st day to the 400th day (January 1–March 11), the calculations were performed with consideration for variations in the Sun's zenith angle. Such a gradual introduction of daily warming variations and the additional equation on the 121st, 122nd, through the 130th days made it possible to obtain the ensembles of the fields of hydrodynamic quantities, which consist of ten model realizations calculated with different initial conditions.

2.3. Methods of Data Processing

Zonally averaged values of air temperature and zonal wind component were analyzed and compared based on model calculations and observational data. Both trends and high-frequency oscillations were eliminated using moving average windows of 10 and 30 days [21]. For a convenient comparison of variations within different latitudinal zones, time series were normalized to the difference between maximum and minimum values. Let us denote the zonally averaged temperature and zonal wind component (obtained after data processing) by T^* and U^*, respectively. Then both U^* and T^* distributions were plotted on the latitude–time and height–time diagrams. These latter and the curves of cross-correlations between U^* and T^* variations within different latitudinal zones and at different atmospheric heights were plotted to analyze the propagation of disturbances vertically and meridionally.

3. CALCULATION RESULTS

3.1. Horizontal Transport

Figure 1 gives an example of time variations in both U^* and T^* distributions at a level of 10 hPa (~30 km) according to observational data for winter 2017 (on the right) and model calculations (on the left) for one of the realizations for the QBO western phase. The bottom graphs show the variations in zonally averaged temperature in the polar region. Two episodes of stratospheric warmings are pronounced in late January and late February.

Good qualitative agreement is seen between model calculations and observational data. In both cases, the

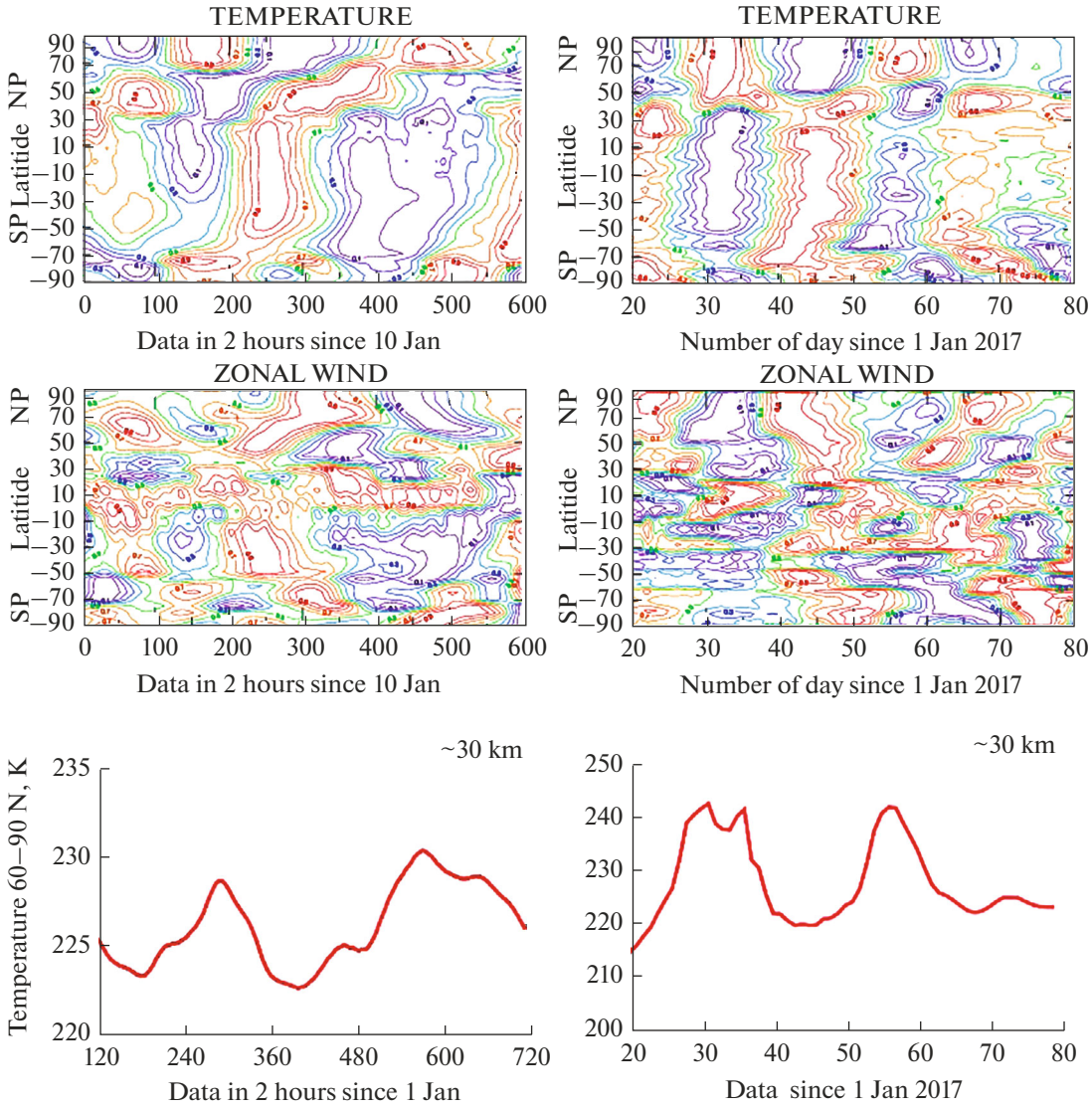

Fig. 1. Latitude–time diagrams for the T^* and U^* distributions according to MUAM (on the left) and ERA-Interim (on the right) data. The graphs (at the bottom) of variations in the zonally averaged air temperature in the polar region according to the MUAM (on the left) and ERA-Interim (on the right) data.

15- to 30-day oscillations are of global character and they are not limited by only the high latitudes of the Northern Hemisphere. In the Southern Hemisphere, the disturbances reach ~50° S according to observational data and ~70° S according to model calculations. Torsional oscillations propagating in the meridional direction are a portion of these disturbances. Such torsional oscillations are well-pronounced within a latitude interval of 30°–60° N according to both observational and model data. Transports between different latitudinal zones are less pronounced in the T^* variations; here, synchronous oscillations (in phase or antiphase) that occupy extended latitudinal zones dominate. The T^* variations are similar to temperature fluctuations in convective cells with upward and downward motions alternating in time. The boundary lines of upward and downward motions coincide with the average climatic position of jet streams.

The abovementioned features are characteristic of all realizations of model calculations and observational data obtained in different years. This is supported by the correlation coefficients (see Figs. 2–9) calculated with a shift of –40 to +40 days between time variations in T^* and U^* within different latitudinal zones at heights of ~30 km (Figs. 2–5) and ~55 km (Figs. 6–9) and averaged over 10 model realizations and the ERA-Interim data over years with different QBO phases. The QBO phases were determined from zonally averaged velocity values for the equator at a level of 10 hPa. The chosen (for calculations) years with the QBO western phase included 1993, 1995, 1997, 1999, 2002, 2004, 2006, 2008, 2011, 2014, and

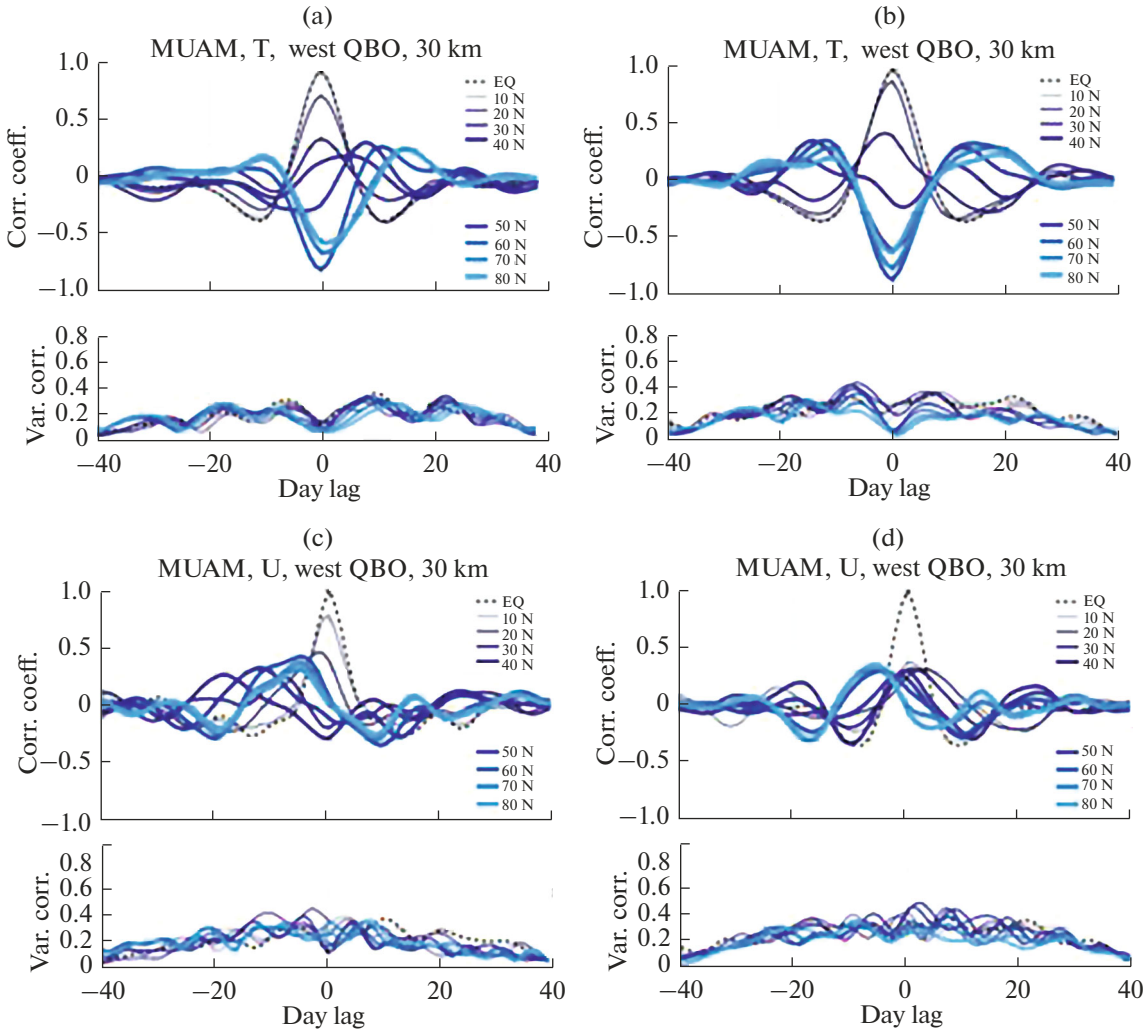

Fig. 2. (Top) Coefficients of correlation between T^* (a, b) and U^* (c, d) variations within different latitudinal intervals, which were averaged over ten model realizations at a height of ~30 km. The left and right graphs correspond to the QBO western and eastern phases, respectively. The dashed curve corresponds to the autocorrelation at the equator; the curves from light blue to dark blue correspond to the coefficients of correlation between the equatorial zone (0° N) and latitudinal zones of 10°, 20°, 30°, 40°, 50°, 60°, 70°, and 80° N. (Bottom) Rms deviations in the correlation coefficients calculated over ten model realizations.

2017 and the years with the QBO eastern phase included 1994, 1998, 2000, 2001, 2003, 2005, 2007, 2010, 2012, and 2015.

On the left, the graphs correspond to the QBO western phase and, on the right, they correspond to the QBO eastern phase. According to all realizations of model calculations and the ERA-Interim data, during both QBO western and eastern phases, the T^* variations within both middle and high latitudes are opposite in sign to those in the low latitudes. The U^* variations within both low and high latitudes are more complex in character: in the high latitudes, these variations are shifted in phase with respect to those in the low latitudes by approximately 5–10 days.

The bottom graphs show the rms deviations of the correlation coefficients. The correlation coefficients exceed the rms deviation within a shift interval of –10 to +10 days and the double rms deviation within a shift interval of –5 to +5 days. This implies that the statistical scatter in individual realizations is insignificant, and the features of the dynamics of the disturbances (which are shown in the diagrams) are characteristic of all realizations.

The differences between the graphs of the correlation coefficients at heights of 30 and 55 km are insignificant. The basic feature of the T^* variations is that the anticorrelation of disturbances within both low and high latitudes is the same at different heights according to both model and observational data. The evidence of the transport of disturbances in the meridional direction is seen in the intermediate latitudinal zones; however, these conclusions are not quite reliable, because the amplitude of such variations with increasing shift most often does not exceed the rms

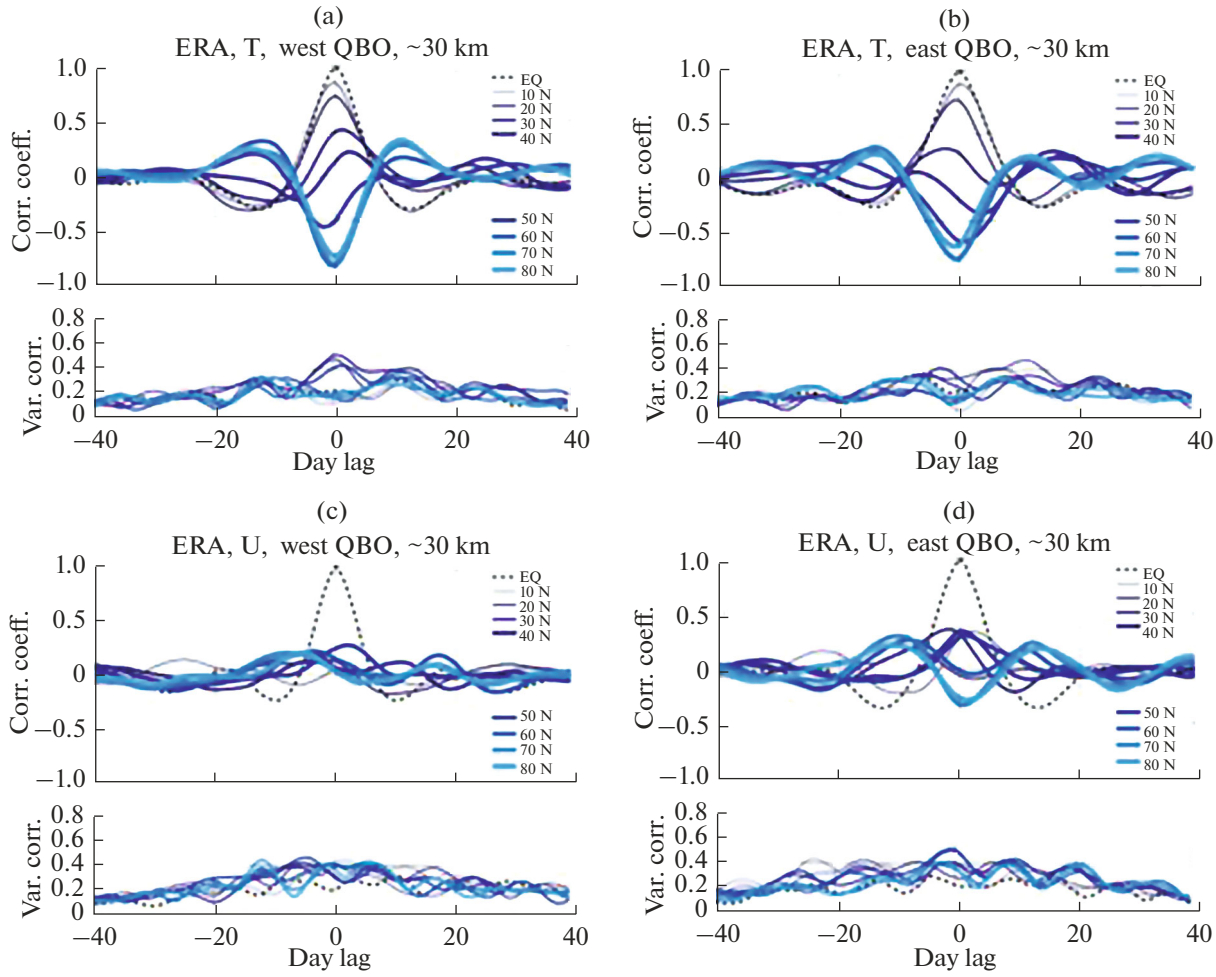

Fig. 3. Same as in Fig. 2, but according to the ERA-Interim data.

deviation. Note that the correlations between variations in different latitudinal zones are not limited by only one hemisphere, which is supported by the diagrams given in Fig. 1 and the graphs of the correlation coefficients given in Fig. 6. Figure 6 shows the distributions of the coefficients of correlation between the T^* variations at the equator and those within latitudinal zones of 80° N to 80° S at a height of ~30 km. The correlation coefficients were calculated individually for the winter–spring and summer periods. In winter of the Northern Hemisphere, the graphs demonstrate the already known T^* anticorrelation between the high and low latitudes. However, the air temperature varies within a latitudinal zone of 0°–40° S synchronously with its variations at the equator; i.e., its variations cover both the Northern and Southern hemispheres.

In summer, such variations are also global; however, the character of their relations is different: synchronous T^* variations within a latitudinal zone of ~0°–40° N anticorrelate with T^* variations within a latitudinal zone of 40°–80° S. If the fact that, in summer, there are no sudden stratospheric warmings in both the Northern and Southern hemispheres is taken into account, one can state that the regularities found in these variations relate to the background characteristics of circulation in the middle atmosphere.

Unfortunately, the features of the filtering method used do not make it possible to estimate the regions of generation and propagation of oscillations. Normalizing time series to differences between maximum and minimum values eliminates any information on oscillation amplitudes in different latitudinal zones. In order to fill this gap, at least, partially, we have analyzed latitudinal variations in differences between maximum and minimum values in the time series of zonally averaged temperature and velocity. If the time series are limited by seasonal intervals, then the maximum and minimum values of the series will most likely be neighboring or corresponding to one and the same phenomenon; however, there remains some probability that their maxima and minima correspond to different events. The role of these differences decreases in averaging over different years.

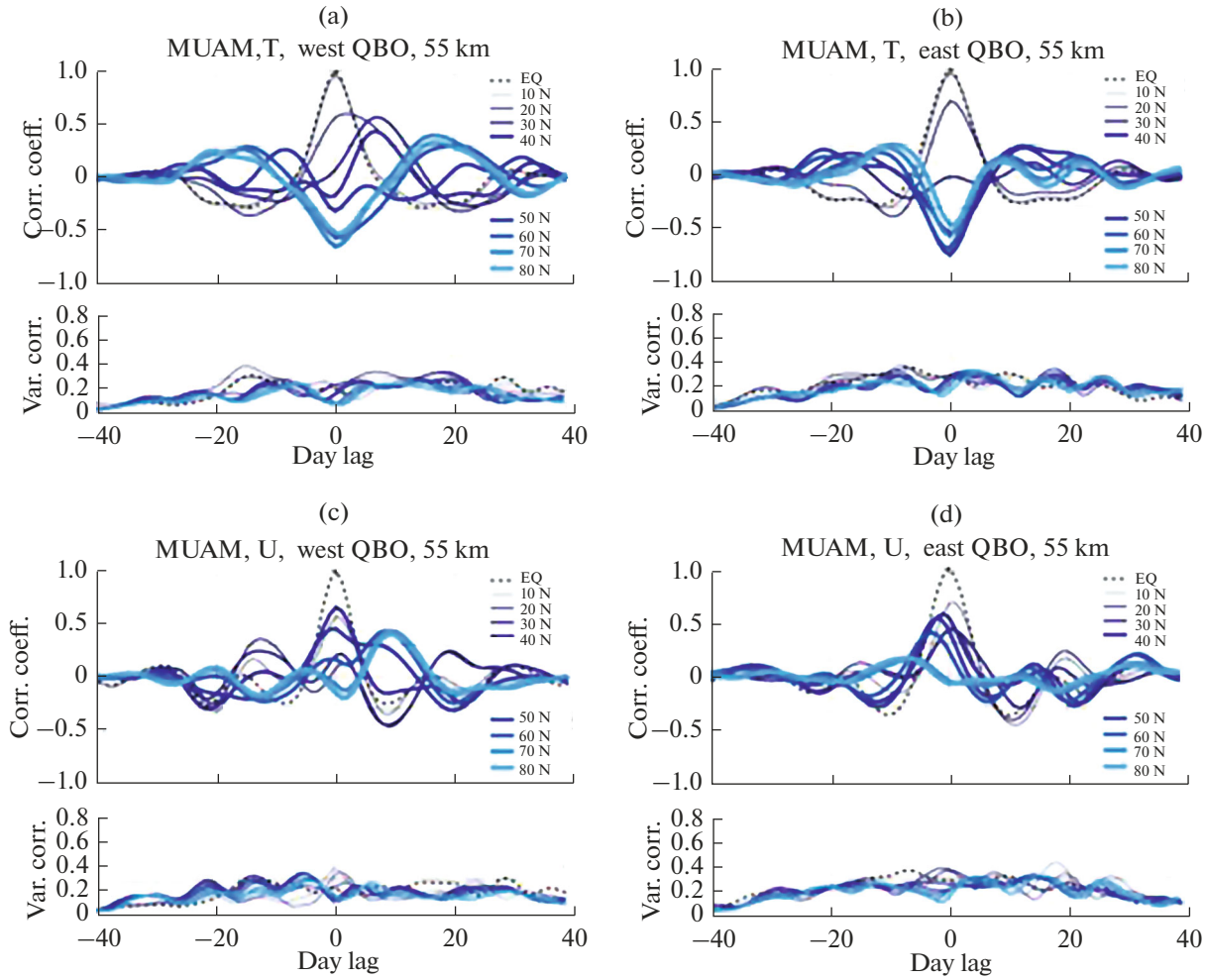

Fig. 4. Same as in Fig. 2, but at a height of ~55 km.

Figure 7 gives the graphs of latitudinal variations (at a level of 10 hPa) in differences between maximum and minimum time series of zonally averaged temperature (dashed curve) and velocity (solid curve) over 140 days beginning from January 1. These graphs are averaged over 20 years from 1997 to 2017. The curves have characteristic inflections that are especially pronounced in normalizing to the latitude-circle length. Figure 7 gives the curves normalized to the latitude-circle length for zonally averaged temperature (red) and velocity (blue) reduced to latitude 40° N. One can expect that, within latitudinal zones without intensified or damped oscillations, the normalized quantities will be represented graphically in the form of straight lines, and for zones in which oscillations intensify (damp), the difference values will increase (decrease). The graphs of rms deviations (thin lines) are plotted to estimate the validity of the variations.

Analyzing Fig. 7, one can see that the high latitudes with maxima at latitudes of approximately 70–80° are a possible region of oscillation generation. This is easily seen in the graphs of the differences between maximum and minimum temperatures and in the graphs of zonally averaged velocity variations. The variations within this region exceed rms deviations and, thus, they are most likely real. Within a latitudinal zone of 40°–60° N, the variation amplitudes have a second, less pronounced maximum; a slight increase in the vicinity of the equator; and a maximum within latitudes of 50°–60° S, but only for zonally averaged velocity.

It should be noted that, unlike the troposphere, in the stratosphere, variations in the zonally averaged quantities are more difficult to interpret, because, in winter, parallel with the polar vortex, one or a few anticyclonic vortices are formed in both the stratosphere and mesosphere. The interaction of these formations determines the dynamics of circulation in the middle atmosphere during SSWs. It is difficult to diagnose this dynamics only on the basis of zonally averaged values. Therefore, in addition, the Fourier series expansions of values along latitude circles are usually used. For comparison, Fig. 8 gives the graphs of the differences in zonally averaged velocity (blue solid curve) and temperature (red dashed curve) values,

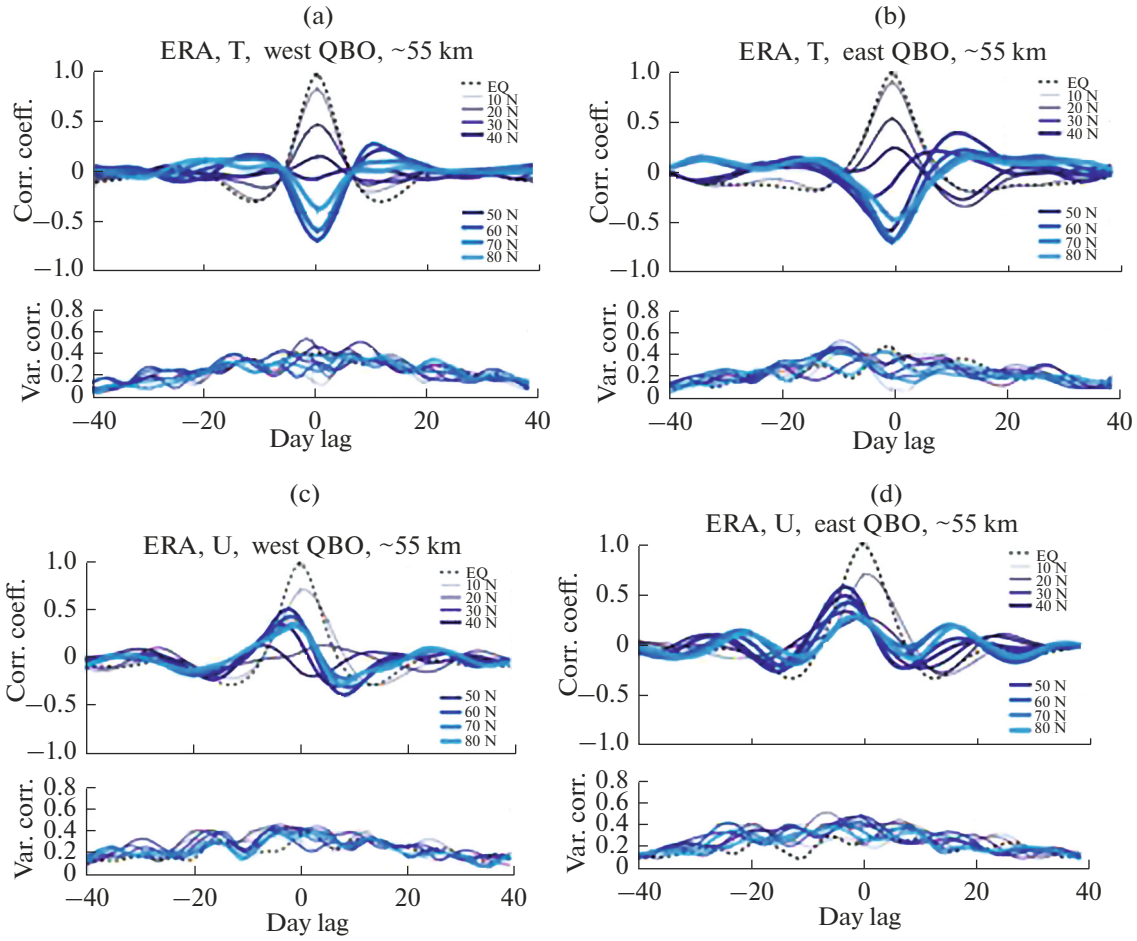

Fig. 5. Same as in Fig. 3, but according to the ERA-Interim data.

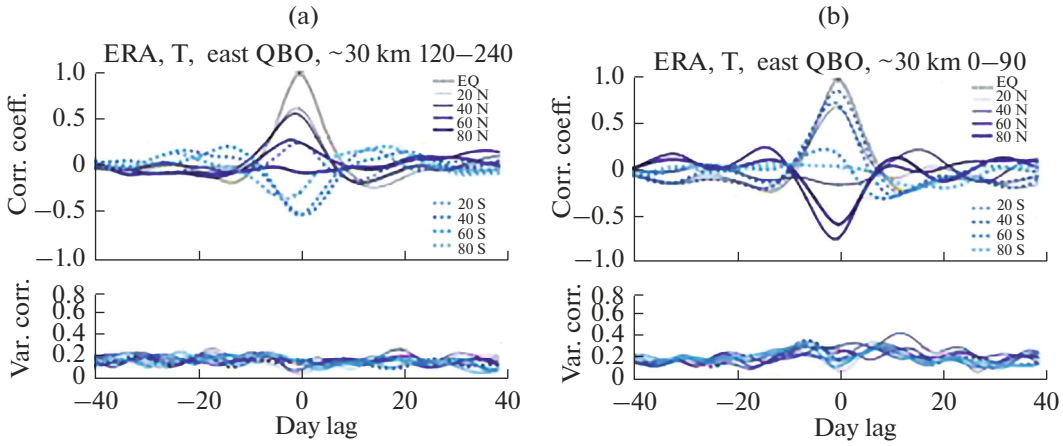

Fig. 6. Distributions of the coefficients of correlation between T^* variations at the equator and those within latitudinal zones of 80° N to 80° S at a height of ~30 km. The correlation coefficients were calculated individually for the winter–spring (on the right) and summer (on the left) periods.

which are similar to the graphs in Fig. 7, but for a level of 500 hPa. It is seen that the amplitude of the variations in zonally averaged velocity and temperature is smaller at this level than in the stratosphere. In this case, maximum temperature variations and, to a lesser degree, zonally averaged velocity variations are shifted (when compared to the stratosphere) toward the middle latitudes. Maximum oscillation generation occurs

at a latitude of approximately 40°, i.e., in the region of a subtropical jet stream. In the Southern Hemisphere, the amplitude of temperature variations increases approximately to 50° S and then decreases. The amplitude of zonally averaged velocity variations remains constant to this latitude circle and, further southwards, also rapidly decreases.

Although the mechanism of exciting oscillations is not clear, such an increase in the oscillation amplitude in the subtropical jet-stream region in the troposphere and in the vicinity of the polar vortex in the middle atmosphere seems quite natural. In fact, both baroclinic and barotropic instabilities are most likely to develop precisely in these regions, and it is in these regions where the storage of available liable energy is maximum. The character of the variations in zonally averaged velocity and temperature makes it possible to assume that their variations reflect natural global oscillations rather than oscillations caused by localized sources. This assumption relates to a greater extent to circulation in the middle atmosphere than in the troposphere.

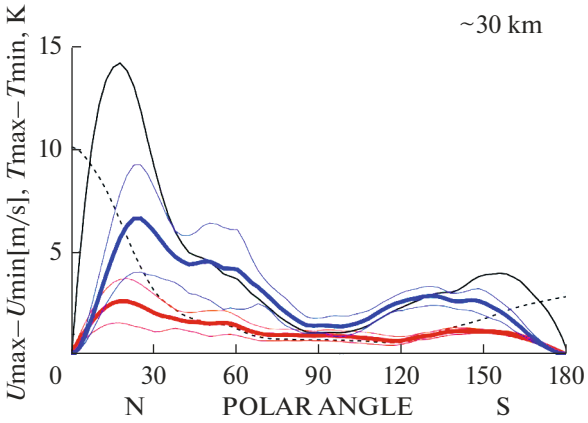

Fig. 7. Graphs of the latitude dependence of the differences between maximum and minimum time series of zonally averaged temperature (dashed curve) and velocity (solid curve) over 140 days beginning from January 1 at a level of 10 hPa. The curves normalized to the length of latitude circles correspond to zonally averaged temperature (red) and velocity (blue) reduced to latitude 40° N.

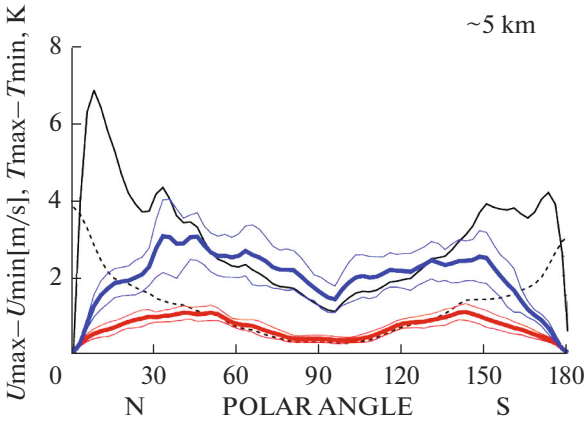

Fig. 8. Same as in Fig. 7, but at a level of 500 hPa.

3.2. Vertical Transport

The fact established on the basis of analyzed observational data is that, during SSWs, temperature disturbances propagate in a downward direction (from the mesosphere to the stratosphere); in this case, the signs of temperature variations for the mesosphere and the stratosphere are most often opposite [4]. This feature is supported by model calculations; moreover, it turns out that the character of variations depends on the QBO phase [14].

To analyze the vertical dynamics of the processes in more detail, we have plotted the T^* and U^* distributions in the height–time diagrams within a latitudinal zone of 60°–90° N for both the QBO western and eastern phases. Figure 9 gives an example of the diagrams for two arbitrarily chosen realizations of model calculations. The range of vertical levels covers the stratosphere, mesosphere, and lower thermosphere.

In the mesosphere, the transport of disturbances in a downward direction is easily seen in the T^* and U^* distributions. In the stratosphere, one can see motions in both downward and upward directions; however, upward motions dominate in temperature and downward motions dominate in zonally averaged velocity. The character of motions is the same during both the QBO western and eastern phases. Opposite signs of temperature disturbances in the stratosphere and mesosphere are the main feature of the T^* distributions. This feature is observed in all realizations of model calculations. Figure 10 shows the distributions of the coefficients of correlation between time variations in T^* (top) and U^* (bottom) within a latitudinal zone of 60°–90° N at different atmospheric heights with respect to variations (at a height of 35 km), which were averaged over ten model realizations. The graphs correspond to the QBO western (on the left) and eastern (on the right) phases.

In the graphs of the correlation coefficients, the main feature of the distribution of T^* variations is easily seen—their opposite character in the mesosphere and stratosphere; moreover, in the mesosphere, the shift of the correlation curves corresponding to different heights implies the downward transport of disturbances for both the QBO western and eastern phases. Within an interval of time shifts from −10 to +10 days and from −5 to +5 days, the correlation coefficient values exceed the value of rms deviation and doubled rms deviation, respectively.

Figure 11 gives the T^* and U^* correlation curves plotted according to observational data. Unfortunately, the ERA-Interim archive data are limited by a

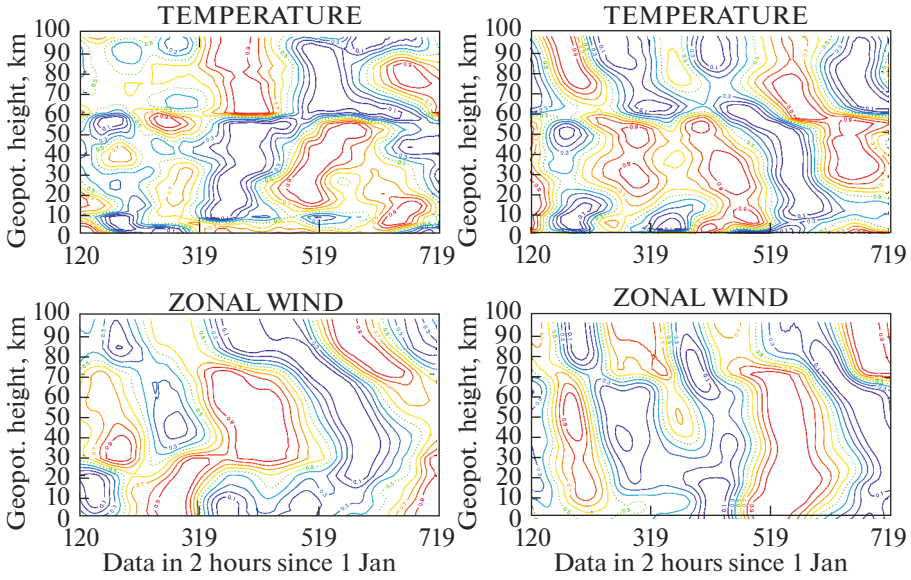

Fig. 9. Vertical T^* and U^* distributions for the QBO western (on the left) and eastern (on the right) phases.

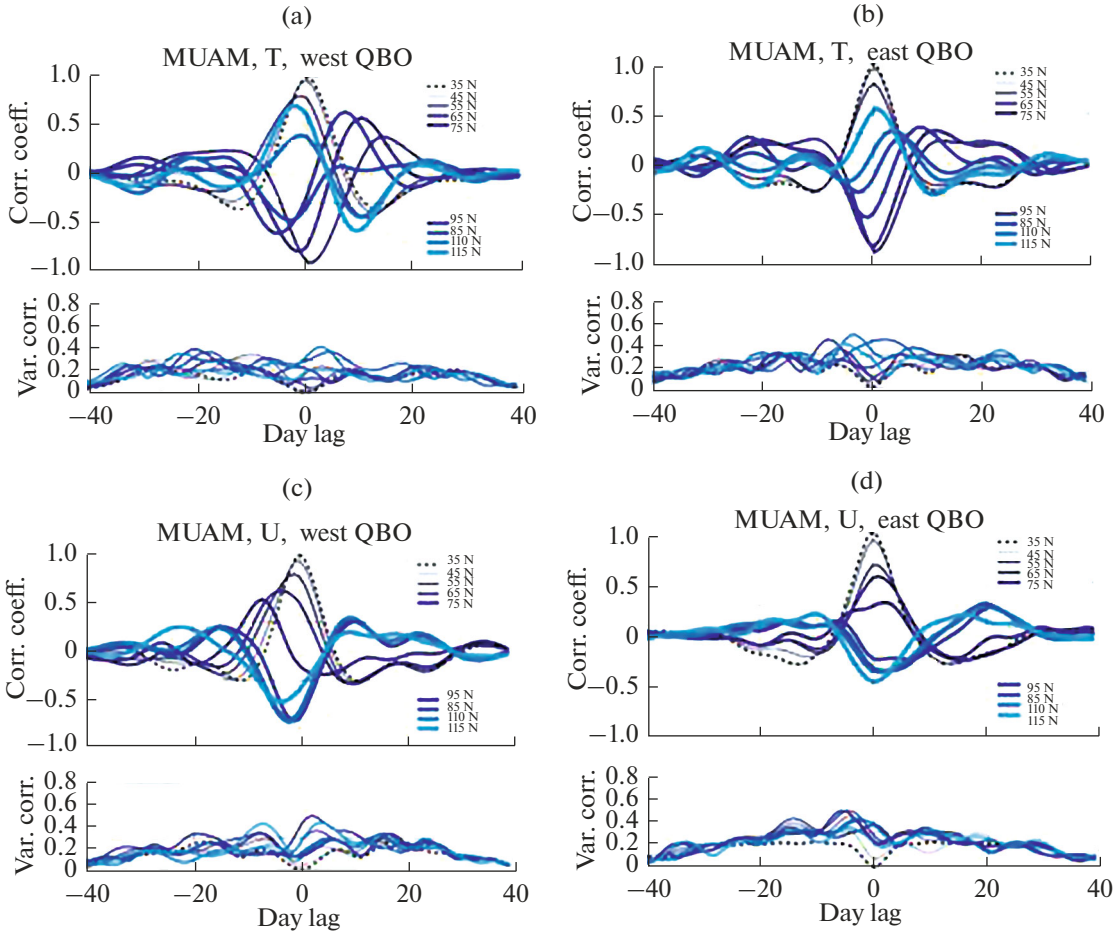

Fig. 10. (Top) Coefficients of correlation (calculated with a shift of –40 to +40 days) between T^* (a, b) and U^* (c, d) time variations at different atmospheric levels with respect to those at a height of 18 km, which were averaged over 10 model realizations. The left graphs correspond to the QBO western phase (a, c) and the right graphs correspond to the QBO eastern phase (b, d). (Bottom) Rms deviations in the correlation coefficients calculated over ten model realizations.

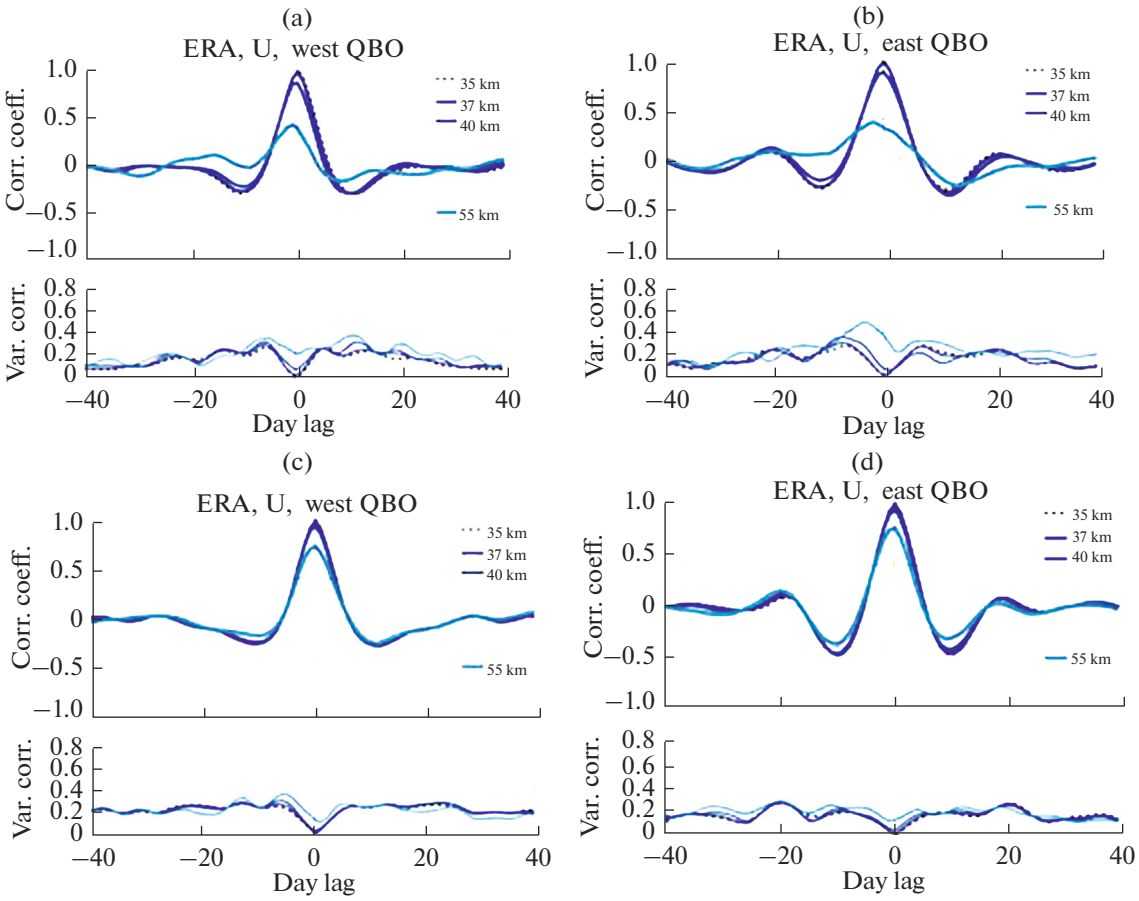

Fig. 11. Curves of correlation between T^* and U^* according to observational data.

level of 0.1 hPa, so in Fig. 11 there are no anticorrelations between temperature variations in the middle atmosphere, which are characteristic of model calculations. However, an agreement up to a height of ~55 km is easily seen between the correlation curves plotted on the basis of model calculations and observational data.

4. DISCUSSION

An analysis of variations in the meteorological parameters of the middle atmosphere showed the presence of global oscillations in both zonally averaged velocity and temperature according to the Era-Interim archive data and model calculations. The scales of oscillations along the meridian amount to tens of degrees; there is agreement between oscillations developed in the Northern and Sothern hemispheres. The vertical oscillation scale is tens of kilometers. The oscillations change their sign in the region of jet streams (and their sign remains unchanged at the equator). The sign of oscillations vertically changes within the stratopause and mesopause; the oscillation period is approximately 10–30 days. Torsional oscillations propagating in a meridional direction are a portion of disturbances. Such torsional oscillations are well-pronounced within a latitude interval of 30°–60° N according to both observational and model data.

According to one of the most common points of view, atmospheric oscillations are a result of both baroclinic and barotropic instabilities, so they may have a structure of the most unstable system eigenmodes. To isolate such oscillations, the method of analyzing equations via linear approximations was proposed by Lyapunov [22]. Such an analysis results in the normal modes of operators characterizing the interaction of disturbances with a mean flow.

The first interpretations of the oscillations in the middle latitudes were reduced to the projection of real disturbances onto the Hough functions and spherical harmonics that are the normal modes of zonally symmetric flows [23–28]. However, the results of comparisons between normal modes and real disturbances were not quite convincing.

The normal modes of differential operators responsible for the interaction of disturbances with the axisymmetric component and both mean-flow and layer-thickness anomalies in a barotropic quasi-geostrophic model are compared in [26]. The normal modes induced by meridional axisymmetric-flow gra-

dients had the smallest increments and long oscillation periods. The mean-flow and layer-thickness anomalies increased the increments by almost an order of magnitude. The characteristic time of the development of instabilities was a few days and the oscillation periods were from 10 days to a few tens of days; disturbances could propagate westward and eastward. The periods, increments, and spatial structure of normal modes were strongly dependent on the structure of mean-flow anomalies and the parameterization of turbulent viscosity.

The unstable normal modes of the climatic January velocity-field distribution at a level of 300 hPa in an evolutionary model with the linear Ekman attenuation and fourth-order viscosity were studied in [27]. Calculations showed that the fastest growing mode had a period of approximately 45 days and the characteristic growth time was 6.8 days in the absence of linear attenuation. During the half-period, the mode development resembled the alternating introduction of action centers with opposite signs over the Pacific and Atlantic. One could see some similarity of the mode obtained with the Arctic Oscillation and the propagation of alternating-sign disturbances from the pole towards Central Asia.

Let us summarize the results obtained from the studies of eigenmodes in hydrodynamic flows. No direct evidence of the existence of zonally symmetric oscillations was obtained. It was found that normal modes strongly depend on the form and amplitude of mean-flow anomalies and viscosity parameterization. However, in this case, some normal modes demonstrated the dynamics whose features, being zonally averaged, could be interpreted as the propagation of torsional oscillations in a meridional direction and changes in the sign of meteorological-parameter anomalies within extended latitudinal zones. Thus, despite the absence of direct evidence of the existence of eigenmodes in large-scale flows on the sphere which have a zonal symmetry, one should not completely abandon this hypothesis.

However, another assumption, that the isolated oscillations are a result of well-known low-frequency normal modes propagating in a zonal direction eastward or westward, is more probable. Interacting with zonal mean-flow inhomogeneities in the stratomesosphere or in the upper troposphere, these modes may generate secondary disturbances propagating in the meridional direction and having periods corresponding to normal modes. A high probability of such an interpretation is supported by the fact that the model includes the parameterization of the basic atmospheric normal modes with periods of 5, 10, and 16 days through the specification of additional warming sources (localized in the troposphere), whose latitudinal structure is specified using the corresponding Hough functions [8].

Determining the spatial structure of meteorological-field variations within a low-frequency range in the middle atmosphere is particularly important in interpreting the oscillations. To solve this problem, one can use natural orthogonal function (NOF) expansions (however, this method is not quite correct because of formally mathematical conditions imposed on the NOFs) or one-point correlations with time shifts. Using these methods in the troposphere has made it possible to discover so-called teleconnections, the interpretation of which is still far from complete.

FUNDING

This work was supported by the Fundamental Research Program II.16.1.1 for State Academies of Sciences (2013–2020), the Russian Foundation for Basic Research (project no. 18-05-01050), and the Russian Science Foundation (project no. 19-77-00009).

REFERENCES

1. J. M. Wallace and M. L. Blackmon, "Observation of low-frequency atmospheric variability," in *Large-Scale Dynamic Processes in the Atmosphere,* Ed. by B. J. Hoskins and R. P. Pearce (Acad. Press, London, 1983).
2. G. Branstator, "The maintenance of low-frequency atmospheric anomalies," J. Atmos. Sci. **49,** 1924–1945 (1992).
3. T. Matsuno, "A model of the stratosphere sudden warming," J. Atmos. Sci. **28,** 1479–1494 (1971).
4. A. Chandran, R. L. Collins, and V. L. Harvey, "Stratosphere-mesosphere coupling during stratospheric sudden warming events," Adv. Space Res. **53,** 1265–1289 (2014).
5. V. Limpasuvan, D. W. J. Thompson, and D. L. Hartmann, "The life cycle of the Northern Hemisphere sudden stratospheric warmings," J. Clim. **17,** 2584–2595 (2004).
6. A. H. Butler, J. P. Sjoberg, D. J. Seidel, and K. H. Rosenlof, "A sudden stratospheric warming compendium," Earth Syst. Sci. Data **9,** 63–76 (2017).
7. A. I. Pogorel'tsev, "Generation of normal atmospheric modes by stratospheric vacillations," Izv., Atmos. Oceanic Phys. **43,** 423–435 (2007).
8. A. I. Pogorel'tsev, E. N. Savenkova, and N. N. Pertsev, "Sudden stratospheric warmings: The role of normal atmospheric modes," Geomagn. Aeron. (Engl. Transl.) **54** (3), 357–372 (2014).
9. H.-L. Liu and R. G. Roble, "A study of a self-generated stratospheric sudden warming and its mesospheric-lower thermospheric impacts using the coupled TIME-GCM/CCM3," J. Geophys. Res. **107,** 46–95 (2002).
10. O. S. Kochetkova, V. I. Mordvinov, and M. A. Rudneva, "Analysis of the factors affecting the occurrence of stratospheric warming," Opt. Atmos. Okeana **27** (8), 719–727 (2014).
11. J. O. Dickey, M. Ghil, and S. L. Marcus, "Extratropical aspects of the 40–50 day oscillation in length-of-day and atmospheric angular momentum," J. Geophys. Res. **96,** 22643–22658 (1991).

12. F. Lott, A. W. Robertson, and G. Michael, "Mountain torques and Northern Hemisphere low-frequency variability. Part I: hemispheric aspects," J. Atmos. Sci. **61,** 1259–1274 (2004).
13. K. Weickmann and E. Berry, "The tropical Madden-Julian oscillation and the global wind oscillation," Mon. Weather Rev. **137,** 1601–1614 (2009).
14. K. K. Kandieva, O. G. Aniskina, A. O. Pogoreltsev, O. S. Zorkaltseva, and V. I. Mordvinov, "Effect of Madden-Julian oscillation and quasi-biennial oscillation on the dynamics of extratropical stratosphere," Geomagn. Aeron. (Engl. Transl.) **59**, 105–114 (2019).
15. A. I. Pogoreltsev, A. A. Vlasov, and Ch. Jacobi, "Planetary waves in coupling the lower and upper atmosphere," J. Atmos. Sol.-Terr. Phys. **69,** 2083–2101 (2007).
16. N. M. Gavrilov and A. V. Koval, "Parameterization of mesoscale stationary orographic wave forcing for use in numerical models of atmospheric dynamics," Izv., Atmos. Oceanic Phys. **49,** 244–251 (2013).
17. E. N. Suvorova, E. A. Drobashevskaya, and A. I. Pogorel'tsev, "Climatic three-dimensional ozone distribution model based on MERRA reanalysis data," Uch. Zap. Ros. Gos. Gidrometeorol. Univ., No. 49, 38–46 (2017).
18. T. S. Ermakova, I. A. Statnaya, I. N. Fedulina, E. V. Suvorova, and A. I. Pogoreltsev, "Three-dimensional semi-empirical climate model of water vapor distribution and its implementation to the radiation module of the middle and upper atmosphere model," Russ. Meteorol. Hydrol. **42,** 594–600 (2017).
19. S. Kobayashi, Y. Harada, Y. Ota, et al., "The JRA-55 reanalysis: General specifications and basic characteristics," J. Meteorol. Soc. Jpn. **93,** 548 (2015).
20. M. M. Rienecker, M. J. Suarez, R. Gelaro, et al., "MERRA: NASA's modern-era retrospective analysis for research and applications," J. Clim. **14,** 3624–3648 (2011).
21. O. S. Zorkaltseva, V. I. Mordvinov, E. V. Devyatova, and N. S. Dombrovskaya, "Method for calculating torsional oscillations in Earth's atmosphere from NCEP/NCAR, MERRA-2, ECMWF ERA-40, and ERA-INTERIM," Sol.-Terr. Phys. **5** (1), 69–76 (2019).
22. *Computational Processes and Systems: Collected Works,* Ed. by G. I. Marchuk (Nauka, Moscow, 1986) [in Russian].
23. V. P. Dymnikov, *Selected Chapters of Stability Theory for the Dynamics of a Two-Dimensional Incompressible Fluid* (Inst. Vych. Matem. Ross. Akad. Nauk, Moscow, 2004) [in Russian].
24. R. Madden, "Observations of large-scale traveling Rossby waves," Rev. Geophys. Space Phys. **17,** 1935–1949 (1979).
25. M. Salby, "A ubiquitous wavenumber 5 anomaly in the Southern Hemisphere during FGGE," Mon. Weather Rev. **110,** 1712–1720 (1982).
26. A. J. Simmons, J. M. Wallace, and G. M. Branstator, "Barotropic wave propagation and instability, and atmosphere teleconnection patterns," J. Atmos. Sci. **40** (6), 1363–1392 (1983).
27. G. M. Branstator, "A striking example of the amosphere's leading traveling pattern," J. Atmos. Sci. **44,** 2310–2323 (1987).
28. V. I. Mordvinov, E. V. Devyatova, and V. M. Tomozov, "Hydrodynamic instabilities in the tachocline, driven by layer thickness variations and mean flow inhomogeneities," Soln.-Zem. Fiz., No. 23, 3–12 (2013).

Translated by B. Dribinskaya